PCCP

PAPER

View Article Online
View Journal | View Issue

Cite this: *Phys. Chem. Chem. Phys.*, 2024, **26**, 19105

Oxygen sensitivity of [FeFe]-hydrogenase: a comparative study of active site mimics inside *vs.* outside the enzyme†

Shanika Yadav, [a] Rieke Haas,[b] Esma Birsen Boydas,[c] Michael Roemelt, [c] Thomas Happe, [b] Ulf-Peter Apfel *[ad] and Sven T. Stripp *[e]

[FeFe]-hydrogenase is nature's most efficient proton reducing and H_2-oxidizing enzyme. However, biotechnological applications are hampered by the O_2 sensitivity of this metalloenzyme, and the mechanism of aerobic deactivation is not well understood. Here, we explore the oxygen sensitivity of four mimics of the organometallic active site cofactor of [FeFe]-hydrogenase, $[Fe_2(adt)(CO)_{6-x}(CN)_x]^{x-}$ and $[Fe_2(pdt)(CO)_{6-x}(CN)_x]^{x-}$ (x = 1, 2) as well as the corresponding cofactor variants of the enzyme by means of infrared, Mössbauer, and NMR spectroscopy. Additionally, we describe a straightforward synthetic recipe for the active site precursor complex $Fe_2(adt)(CO)_6$. Our data indicate that the aminodithiolate (adt) complex, which is the synthetic precursor of the natural active site cofactor, is most oxygen sensitive. This observation highlights the significance of proton transfer in aerobic deactivation, and supported by DFT calculations facilitates an identification of the responsible reactive oxygen species (ROS). Moreover, we show that the ligand environment of the iron ions critically influences the reactivity with O_2 and ROS like superoxide and H_2O_2 as the oxygen sensitivity increases with the exchange of ligands from CO to CN^-. The trends in aerobic deactivation observed for the model complexes are in line with the respective enzyme variants. Based on experimental and computational data, a model for the initial reaction of [FeFe]-hydrogenase with O_2 is developed. Our study underscores the relevance of model systems in understanding biocatalysis and validates their potential as important tools for elucidating the chemistry of oxygen-induced deactivation of [FeFe]-hydrogenase.

Received 12th December 2023,
Accepted 25th June 2024

DOI: 10.1039/d3cp06048a

rsc.li/pccp

Introduction

Renewable energy sources such as solar, wind, and hydropower offer sustainable alternatives to fossil fuels but suffer from limitations in storage and transportation, impelling researchers to look for other sources of energy. Molecular hydrogen (H_2) is a promising clean energy storage and transport molecule;[1–4] however, cost-efficient and sustainable generation of H_2 is yet to be achieved. Biotechnological H_2 generation *via* the enzyme hydrogenase[5] is one potential pathway to produce "green fuel". Although [NiFe]- and [FeFe]-hydrogenases are amongst the most effective H_2-forming enzymes (TOF of up to $\sim$21 000 s^{-1}),[6–8] biocatalytic H_2 production is at a very early technology readiness level.

The efficiency of [FeFe]-hydrogenases is attributed to their organometallic cofactor. The so-called H-cluster is an assembly of two distinct iron–sulfur sites connected *via* a cysteine ligand: a [4Fe–4S] cluster, which participates in electron transfer during catalysis and a unique diiron site, where the proton reduction reaction occurs (Fig. 1). The H-cluster carries an "azadithiolate" ligand (adt) and two μCO-bridged iron ions, each of which is coordinated additionally to a terminal CN^- and CO ligand. Fig. 1 illustrates how the cyanide ligands may interact with residues in the active site.[9] The adt ligand functions as an internal hydrogen-bonding donor and proton relay site, coupling proton transfer across the protein fold to an open coordination site at the distal iron ion (Fe_d) of the diiron site.[10] The proton transfer pathway comprises cysteine, glutamic acid,

[a] *Inorganic Chemistry I, Ruhr-Universität Bochum, Universitätsstraße 150, 44801 Bochum, Germany. E-mail: ulf.apfel@rub.de*
[b] *Faculty of Biology & Biotechnology, Ruhr-Universität Bochum, Universitätsstrasse 150, 44801 Bochum, Germany*
[c] *Institute of Chemistry, Humboldt-Universität zu Berlin, Brook-Taylor Str.2, 12489, Berlin, Germany*
[d] *Department of Electrosynthesi, Fraunhofer UMSICHT, Osterfelder Str. 3, 46047 Oberhausen, Germany*
[e] *Biophysical Chemistry, Technical University Berlin, Strasse des 17. Juni 124, 10623 Berlin, Germany. E-mail: s.stripp@tu-berlin.de*

† Electronic supplementary information (ESI) available. See DOI: https://doi.org/10.1039/d3cp06048a

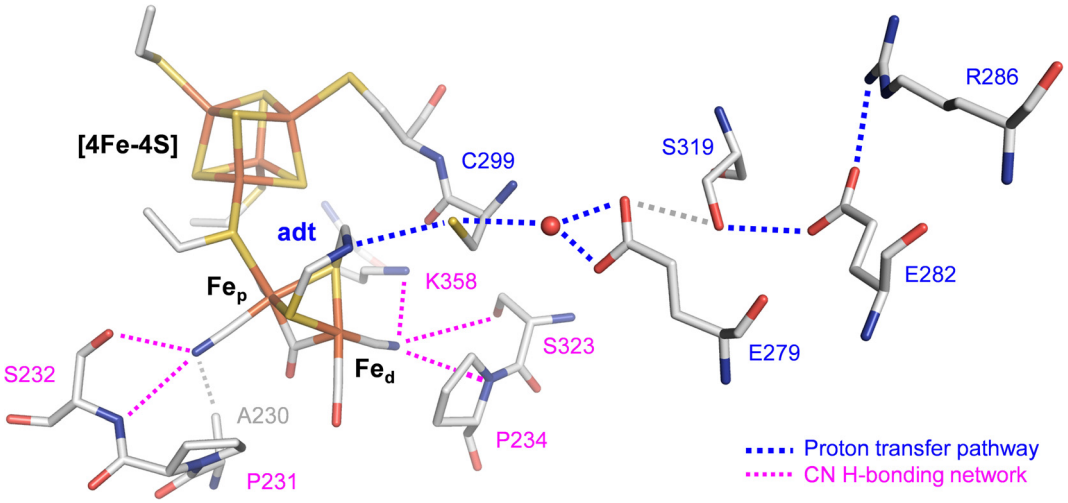

Fig. 1 Stick representation of the active site and the proton transfer pathway (PTP) of [FeFe]-hydrogenase *Cp*I (PDB ID 4XDC).[11] The H-cluster consists of a [4Fe–4S] cluster connected to a diiron site with an open site at Fe_d where O_2, H_2, or CO can bind. *Via* the azadithiolate ligand (adt), the H-cluster exchanges protons with the PTP (blue traces) that connects active site and bulk solvent. The cyanide ligands of the H-cluster are hydrogen-bonded to residues in the 2nd coordination sphere (magenta traces).

serine, and arginine residues (Fig. 1). Despite their catalytic efficiency, large-scale applications are limited due to the O_2 sensitivity of [FeFe]-hydrogenase. Investigating the mechanism of aerobic deactivation is crucial for understanding and addressing these challenges and will inspire strategies of enhancing enzyme stability and functionality in the presence of O_2 expanding the applicability of [FeFe]-hydrogenases.

To understand the reaction of [FeFe]-hydrogenase with O_2, numerous theoretical and spectroscopic studies have shown diffusion of O_2 through hydrophobic gas channels.[12–14] We and others have suggested that O_2 undergoes reductive activation at the H-cluster and is converted to reactive oxygen species (ROS), which subsequently damage the diiron site, the [4Fe–4S] cluster, or both.[15–18] In addition, CO inhibition experiments revealed that CO shields the H-cluster against aerobic deactivation suggesting that Fe_d is the initial binding site for both O_2 and H_2 (Fig. 1).[17–19] In similar fashion, the [FeFe]-hydrogenase *Cb*A5H is protected from aerobic deactivation by interconversion from the H_{ox} state to the sulfur-inhibited H_{intact} state in the presence of O_2.[20–22] Another mechanism applies to the sensory [FeFe]-hydrogenase *Tam*HydS that forms a stable intermediate due to insufficient proton transfer as a sub-step in the reaction with O_2.[23,24] Oxygen tolerance (*i.e.*, hydrogen turnover in the presence of O_2) and a catalytic reduction of O_2 to water like in certain [NiFe]-hydrogenases[25–29] has not been observed with [FeFe]-hydrogenase.

With respect to synthetic mimics of the H-cluster, past research was focused on studying the reaction of carbonyl-type diiron complexes with O_2 or ROS. However, there has been a lack of investigation into the oxygen reactivity of $[Fe_2(xdt)(CO)_4(CN)_2]^{2-}$ type complexes. This may be due to the demanding synthesis of such compounds. For example, the synthetic route towards model complex $[Fe_2(adt)(CO)_4(CN)_2]^{2-}$ involves condensation of $Fe_2(SH)_2(CO)_6$ with premixed solution of $(NH_4)_2CO_3$ and paraformaldehyde to afford the diiron azadithiolate precursor $Fe_2(adt)(CO)_6$, which renders the desired mimic after CO/CN^- ligand exchange ready to be inserted in hydrogenase apoenzyme ("artificial maturation").[30–33] Despite the widespread utilization of this protocol, the process suffers from several challenges. For example, the yields of $Fe_2(adt)(CO)_6$ have been low and inconsistent. Additionally, the use of $Fe_2S_2(CO)_6$, which is acquired through a challenging synthetic pathway, further undermines the appeal of this method.[31,34,35] Addressing these obstacles, we herein describe a straightforward and scalable synthetic scheme for the precursor complex $Fe_2(adt)(CO)_6$ (Fig. S1, ESI†).

Previously, several diiron site mimics have been investigated towards their proton reduction mechanism, while only a few reports highlight the reactivity with O_2.[7,36–39] For example, Darensbourg *et al.* reported on the site-specificity of the oxygenation of $Fe_2(pdt)(CO)_{6-x}(L)_x$ (pdt = $S_2(CH_2)_3$, L = CO, PMe_3, PPh_3; x = 1 or 2) with *m*-chloroperoxybenzoic acid. Although density functional theory (DFT) calculations suggested formation of a Fe–O–Fe bond species, experimental studies revealed a dithiolate-centred oxidation, resulting exclusively in S-oxygenated reaction products.[39] Similarly, Weigand *et al.* reported on the chemical sulfur oxidation of $Fe_2(sdt)(CO)_6$ type models with varying equivalents of dimethyldioxirane (sdt = $S_2(CH_2)_2S$).[38,40] Furthermore, Dey *et al.* reported hexacarbonyl diiron mimics with a 4-bromoaniline dithiolate ligand that electrocatalytically convert O_2 at reducing potentials.[36] Here, formation of H_2O_2 was observed and the bridgehead amine was suggested to be of key importance to protect these H-cluster mimics from further aerobic deactivation. Along these lines, Berggren and Hammerström *et al.* conducted oxidative studies on the hexacarbonyl diiron mimics $Fe_2(adt)(CO)_6$ and $Fe_2(pdt)(CO)_6$ with O_2 and ROS. Here, the interaction of $Fe_2(adt)(CO)_6$ with O_2 in presence of chemical reductants lead to short-lived species with oxygenated thiol groups.[37]

As the individual steps of cluster degradation remained unidentified, we investigate the oxygen sensitivity of biomimetic

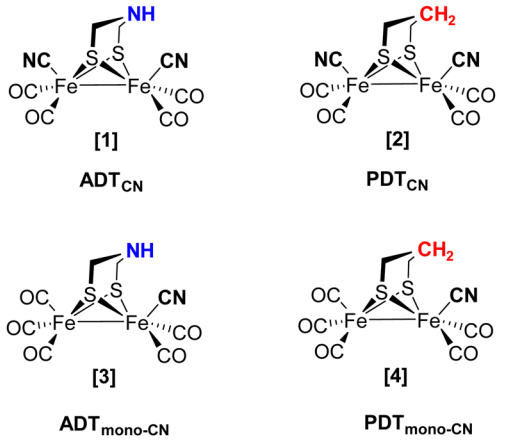

Fig. 2 Schematic drawings of the active site models investigated in this study. Complex **[1]** closely resembles the H-cluster while the natural adt ligand (headgroup NH, blue) is replaced by a pdt ligand in **[2]** (headgroup CH_2, red).

complexes $[Fe_2(adt)(CO)_{6-x}(CN)_x]^{x-}$ and $[Fe_2(pdt)(CO)_{6-x}(CN)_x]^{x-}$ with $x = 2$ (ADT_{CN} **[1]** and PDT_{CN} **[2]**) and $x = 1$ ($ADT_{mono\text{-}CN}$ **[3]** and $PDT_{mono\text{-}CN}$ **[4]**) in this work to receive a deeper understanding of the mechanism of aerobic deactivation in [FeFe]-hydrogenase (Fig. 2). We emphasize that these four active site models are direct mimics of the H-cluster, and ADT_{CN} **[1]** and PDT_{CN} **[2]** are commonly utilized for artificial maturation of [FeFe]-hydrogenase.[30,31]

Among the various oxygen species, superoxide (O_2^-) is the most likely ROS affecting iron–sulfur clusters, and it is a much stronger one-electron oxidant than O_2 (+0.9 V and −0.1 V *vs.* RHE, respectively).[41] Additionally, formation of H_2O_2 is not uncommon in natural systems and considered a harmful substrate for [FeFe]-hydrogenase in particular.[42–44] Following these considerations, we report the interactions of complexes **[1–4]** with O_2, H_2O_2, and superoxide by means of FTIR and Mössbauer spectroscopy, both in the presence and absence of protons. In the next step, model complexes **[1–4]** were probed as part of the H-cluster within the [FeFe]-hydrogenase of *Chlamydomonas reinhardtii*, *Cr*HydA1. Four cofactor variants *Cr*HydA1^{adt}, *Cr*HydA1^{pdt}, *Cr*HydA1$^{mono\text{-}adt}$, and *Cr*HydA1$^{mono\text{-}pdt}$ were spectroscopically investigated towards O_2-induced deactivation. Additionally, *Cr*HydA1^{adt} and *Cr*HydA1^{pdt} variants were treated with H_2O_2. We find that proton transfer and hydrogen-bonding with the adt ligand critically influence the reactivity with O_2 but barely affect H_2O_2-mediated oxidation. Our results facilitate understanding the initial steps of O_2 deactivation in the biological system and show that the model complexes directly reflect the reaction of [FeFe]-hydrogenase with O_2 and ROS.

Materials and methods

Synthesis of $Fe_2(adt^{Cbz})(CO)_6$

Under inert conditions, $Fe_3(CO)_{12}$ (100 mg, 0.20 mmol) was dissolved in 20 ml THF. Then, adt^{Cbz} (58.4 mg, 0.24 mmol) was added dropwise *via* a syringe to the solution. The reaction was refluxed for 2 h, whereby the color of the reaction mixture changed from dark blue to reddish-brown. Afterwards the reaction mixture was allowed to cool to room temperature and the volatiles were removed *in vacuo*. Column chromatography using SiO_2 (DCM : PE 3 : 1) was conducted. The red fraction was collected, dried over $MgSO_4$, filtered, and concentrated. After removal of the solvent *in vacuo* the dark red product was obtained with a yield of 80% (83 mg). Crystals for X-ray diffraction analysis (Fig. S1, ESI†) were grown upon slow evaporation of saturated solution of $Fe_2(adt^{Cbz})(CO)_6$ in pentane at 4 °C. The FTIR spectrum is shown in Fig. S2A (ESI†).

Synthesis of $Fe_2(adt)(CO)_6$ from $Fe_2(adt^{Cbz})(CO)_6$

Under inert conditions, $Fe_2(adt^{Cbz})(CO)_6$ (100 mg, 0.19 mmol) was dissolved in 5 ml DCM. Then, degassed Me_2S (0.37 ml, 5.15 mmol) and $BF_3{\cdot}Et_2O$ (0.48 ml, 48%) were added and the mixture was stirred for 1.5 h at RT until the red solution brightened up a little. Hereafter, additional Me_2S (0.30 ml, 4.20 mmol) was added, and the mixture was allowed to stir for another 2 h at RT. Next, 3.5 ml degassed H_2O was added followed by addition of 3.5 ml 10% NH_4OH. After shortly stirring the mixture, the compound was extracted with 3 × 5 ml DCM. The organic phase was dried over $MgSO_4$ and filtered. After removal of the solvent *in vacuo* the crude product was obtained as reported before.[45] Following column chromatography (SiO_2) DCM : PE 1 : 1, the red fraction was collected, dried over $MgSO_4$ (which was filtered off) and the organic phase was dried *in vacuo* yielding $Fe_2(adt)(CO)_6$ as a red powder with a yield of 60% (44 mg). The FTIR spectrum is shown in Fig. S2B (ESI†).

Synthesis of ADT^{CN} [1] $[Fe_2(adt)(CO)_4(CN)_2][Et_4N]_2$

$Fe_2(adt)(CO)_6$ (0.1 g, 0.26 mmol) was dissolved in CH_3CN (2 ml) and cooled to 0 °C. A cold solution of $[Et_4N][CN]$ (0.085 g, 0.55 mmol) in CH_3CN (1 ml) was introduced *via* a gas-tight syringe to the $Fe_2(adt)(CO)_6$ solution. The reaction mixture instantaneously turned dark red and released CO gas as previously reported.[32] The reaction was allowed to warm to room temperature and further allowed stirring for 3 h. The solvent was removed *in vacuo* to give a dark red residue. The complex was transferred to the glovebox and was washed with 6 ml of diethylether (Et_2O), followed by washing with Et_2O : MeCN (20 : 1). The complex was dried, resulting in the dark red solid (0.113 g, 68%). A similar procedure was followed for the synthesis of PDT^{CN} **[2]** $[Fe_2(pdt)(CO)_4(CN)][Et_4N]_2$ from $Fe_2(pdt)(CO)_6$. See Fig. S3 (ESI†) for a schematic depiction of the synthetic route.

Synthesis of $ADT^{mono\text{-}CN}$ [3] $[Fe_2(adt)(CO)_5(CN)][Et_4N]$

A mixture of $Fe_2(adt)(CO)_6$ (0.1 g, 0.26 mmol) and Me_3NO (0.0195 g, 0.26 mmol) was dissolved in CH_3CN (2 ml) and cooled to −40 °C. A cold solution of $[Et_4N][CN]$ (0.028 g, 0.26 mmol) in CH_3CN (1 ml) was introduced *via* a gas-tight syringe to the $Fe_2(adt)(CO)_6$ + Me_3NO solution. The reaction mixture turned dark red and released CO gas as previously

reported.[46] The reaction mixture was allowed to warm to room temperature and further stirred for 3 h. The solvent was removed *in vacuo* to give a dark blackish red, sticky residue. Inside a glove box, the complex was washed with 6 ml of Et_2O, followed by washing with Et_2O : MeCN (20 : 1). The complex was dried resulting in the dark blackish-red solid with a yield of 62% (0.085 g). Similar procedure was followed for the synthesis of $PDT^{mono\text{-}CN}$ **[4]** $[Fe_2(pdt)(CO)_5(CN)][Et_4N]$ from $Fe_2(pdt)(CO)_6$.

See ESI† for details on further Material and methods.

Results and discussion

Reaction of the complexes with O_2

Under an inert argon atmosphere, complex ADT_{CN} **[1]** and PDT_{CN} **[2]** reveal nearly identical FTIR spectra between 1800–2150 cm^{-1} (Fig. 3). The five observed bands have been assigned to the coupled CN^- and CO stretching vibrations and suggest reduced Fe^I–Fe^I complexes.[47] The response toward O_2 was studied by purging pure oxygen gas through the individual solutions in MeCN. A mean shift of Δ = 96 cm^{-1} and Δ = 92 cm^{-1} towards higher wavenumbers was observed (Table 1) but while the CO and CN^- bands drastically lost intensity for ADT_{CN} **[1]** the overall band intensity of PDT_{CN} **[2]** was less affected.

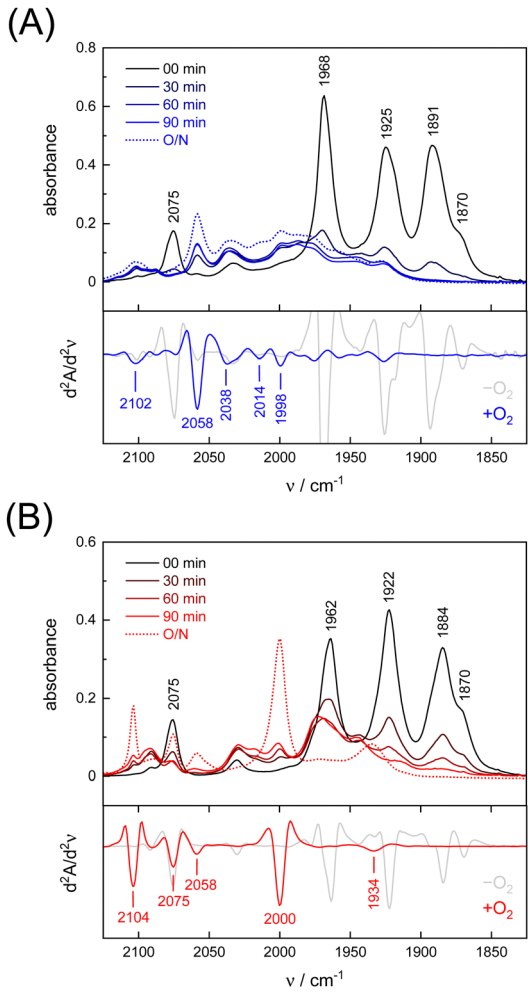

Fig. 3 (A) FTIR spectra of ADT_{CN} **[1]** and (B) PDT_{CN} **[2]** in MeCN upon O_2 purging for 30 seconds, recorded every 30 minutes and after overnight incubation (O/N = 23 h). Below each absorbance spectrum, the second derivative spectrum at 0 min ($-O_2$) and after 23 h ($+O_2$) is plotted to identify the bands of the O_2-oxidised complexes.

Table 1 Observed IR band positions and assignment for complex ADT_{CN} **[1]** and PDT_{CN} **[2]**. The reported values are before and after treatment with O_2 (Δ = band shift)

	[1]	[1]		[2]	[2]	
Model	$-O_2$	$+O_2$	Δ	$-O_2$	$+O_2$	Δ
νCO	1870	1998	**128**	1870	1934	**64**
νCO	1891	2014	**123**	1884	2000	**116**
νCO	1925	2038	**113**	1922	2058	**136**
νCO	1968	2058	**90**	1962	2075	**113**
νCN^-	2075	2102	**27**	2075	2104	**29**
Mean	*1946*	*2045*	***96***	*1943*	*2024*	***92***

The spectrum of O_2-treated complex **[1]** after 90 minutes indicates a number of broad features spanning from 1930–2100 cm^{-1} along with better defined bands at 1998, 2014, 2038, and 2058 cm^{-1} that we assign to the CO ligands. The second derivative FTIR spectrum in Fig. 3(A) suggests a high-frequency band at 2102 cm^{-1} assigned to the CN^- ligands. For complex **[2]**, sharper and more defined CO signals emerge at 1934, 2000, 2058, and 2075 cm^{-1}, with one CN^- band at 2104 cm^{-1} (second derivative FTIR spectrum in Fig. 3(B)), notably only after overnight incubation in the presence of O_2. The reaction with O_2 does not lead to complete loss of CO and CN^- ligands, which is evident from the FTIR spectra measured after up to 23 hours (Fig. S4, ESI†). Interestingly, complex PDT_{CN} **[2]** seems to be particularly O_2-stable. For both complexes, the mean difference in CO/CN^- frequency is small under anaerobic conditions ($-O_2$, Δ = 3 cm^{-1}) but the difference increases under aerobic conditions ($+O_2$, Δ = 21 cm^{-1}) reflecting the ten times stronger up-shift for complex ADT_{CN} **[1]** (Table 1).

Interestingly, we observed that both the nature of the dithiolate head group and the composition of diatomic ligands affect the susceptibility for O_2 damage. Fig. 4(A) shows the intensity of the CO band at 1891 cm^{-1} and 1884 cm^{-1} of the reduced complex **[1]** and **[2]** as a function of time, which allows comparing the decay velocity and illustrates the faster degradation of ADT_{CN} **[1]**. For $ADT_{mono\text{-}CN}$ **[3]** a comparatively slow decrease in band intensity upon exposure to O_2 is observed; however, no oxidized product accumulates. Besides a small loss in intensity, the FTIR spectrum of $PDT_{mono\text{-}CN}$ **[4]** remains largely unaltered under O_2 (Fig. S5, ESI†). These observations are in line with previous reports, which state that complex **[1]** and **[2]** are easier to oxidize than their mono-cyanide derivates.[48]

In variance to earlier observations,[37] no oxygenation of the thiol group were observed, at least within the timeframe of our experiments (Fig. S4, ESI†). The low-frequency end of the IR spectrum below 1200 cm^{-1} is sensitive for S=O vibrations.[49] Instead, we presume that O_2 reacts at the metal sites. While direct spectroscopic evidence of O_2 binding at the metal centers is lacking, the large CO/CN^- band shifts towards higher

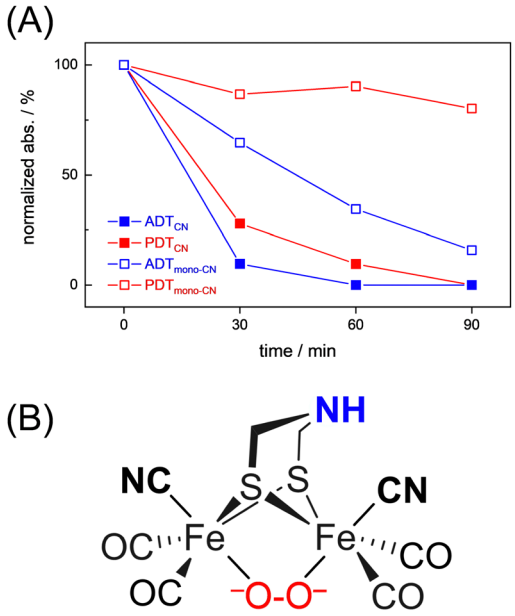

Fig. 4 (A) Comparison of the O_2-induced decay of complexes **[1–4]**. At t_0, the band intensity at 1891 cm^{-1} (ADT_{CN} **[1]**), 1884 cm^{-1} (PDT_{CN} **[1]**), and 1975 cm^{-1} ($ADT_{mono\text{-}CN}$ **[3]** and $PDT_{mono\text{-}CN}$ **[4]**) was normalized to 1 and plotted against time (spectral traces in Fig. 3 and Fig. S5, ESI†). The graph illustrates how the adt-type complexes decay faster than the pdt-type complexes, and how di-cyanide complexes decay faster than mono-cyanide complexes. (B) Most probable structure of a di-ferrous peroxide dianion intermediate of ADT_{CN} according to DFT calculations.

wavenumbers for complex ADT_{CN} **[1]** and PDT_{CN} **[2]** indicates oxidation of the diiron site.

To shed light on the nature of the observed products, a comprehensive density functional theory (DFT) investigation has been conducted. Initial states of the complexes **[1]** and **[2]** with two antiferromagnetically coupled local spins leading to a spin singlet was modelled by means of broken-symmetry DFT. The oxygenation reaction has been explored through three primary routes, as illustrated in Fig. S19 and S20 (ESI†). These routes encompass both terminal and bridging coordination modes, while the latter of which can occur in either ''end-on'' or ''side-on'' fashion. For all different oxygen attack modes, complex **[1]** exhibited lower activation barriers, approximately 2–3 kcal mol^{-1} lower than that of complex **[2]**, confirming the reactive nature of **[1]**. When one electron is transferred from the diiron cluster to O_2, the resulting Fe^{II}–Fe^{I} superoxo complex emerges as a reactive intermediate for both complexes across all conceivable binding modes. According to the modeled reaction mechanism, it was determined that the terminal coordination of oxygen is unlikely. Instead, the thermodynamically favored product contains a peroxide dianion that bridges the two Fe^{II} centers as depicted in Fig. 4(B).

In addition to the aforementioned considerations of the reaction energetics, the calculated CO-stretch frequencies were compared to the experimentally observed IR bands. As depicted in the correlation analysis shown in Fig. S23 (ESI†), formation of a bridging hydride is the most probable form of the protonated compounds, *i.e.*, **[1,2]** + H^+. Results for the oxygenated products, on the other hand, are not as clear and straightforward. The oxygenation at one of the sulfur atoms did not induce a significant difference in the CO/CN-vibration regime compared to the initial XDT_{CN}–O_2 system. This result was anticipated since the coordination environment of the iron centers remains unchanged in this binding mode. Conversely, terminal coordination of the O_2 moiety consistently led to a highly asymmetric shift in CO-vibrations across all cases, which contradicts the experimentally observed differences, as shown in Tables S3 and S4 (ESI†). Considering the reaction profiles alongside the IR data, it can be inferred that terminal binding of oxygen is highly improbable. The bridging coordination of the peroxide dianion to Fe^{II}–Fe^{II} is distinguished by a consistent, progressively positive shift (relative to the initial states) averaging around 90 cm^{-1}. This observed shift, consistent across both experimental data and simulations, aligns closely with the experimental findings. Further details involving the computational methodology, structural isomers (apical-basal) of **[1–2]**, spin isodensity plots depicting the possible intramolecular magnetic exchange interactions, reaction profiles, and an analysis of IR bands can be found in ESI.†

Complexes **[1]** and **[2]** were found to be EPR inactive, both in the absence and presence of O_2 (data not shown). This hints at a two-electron oxidation process, converting a diamagnetic starting state [Fe^{I}–Fe^{I}] into a diamagnetic product state [Fe^{II}–Fe^{II}]. The strong IR up-shift of 92–96 cm^{-1} (Table 1) and the DFT evaluation (Fig. S22, ESI†) agrees with this explanation. In the next step, we analyzed the reaction with O_2 using Mössbauer spectroscopy to demonstrate metal oxidation directly. The MeCN solutions of complex **[1]** and **[2]** were treated with O_2 for 30 seconds. Then, the samples were frozen in liquid nitrogen and measured. Mössbauer spectra (based on the natural abundance of ^{57}Fe) for complex **[1]** and **[2]** after O_2 exposure result in two quadrupole doublets (Fig. 5, bottom traces) that significantly differ from the respective starting materials (Fig. 5, top traces and Table 2).

For both complexes, an increase of isomer shift is observed indicating oxidation from Fe^{I} to Fe^{II}. However, while one site reveals a lower quadrupole splitting and isomer shift (Fe1 in Table 2), the second site shows higher values for both parameters (Fe2 in Table 2) suggesting that the metal centers in both complex **[1]** and **[2]** have a similar oxidation state. This agrees with a formal redox state [Fe^{II}–Fe^{II}]. These measurements demonstrate that iron participates in the reaction with O_2, and that the coordination environment is clearly altered.

The high reactivity of complex **[1]** and **[2]** with O_2 made an isolation of the degradation products challenging. The obtained FTIR and Mössbauer spectra as well as DFT calculations now support the oxidation of the metal centers with subsequent loss of ancillary ligands under aerobic conditions, in particular for the adt-type complexes **[1]** and **[3]**. Such observations have been previously reported for the [FeFe]-hydrogenase *Cr*HydA1, and the formation of superoxide at the H-cluster has been concluded.[17] In a cysteine-to-alanine variant impaired for proton transfer, the corresponding

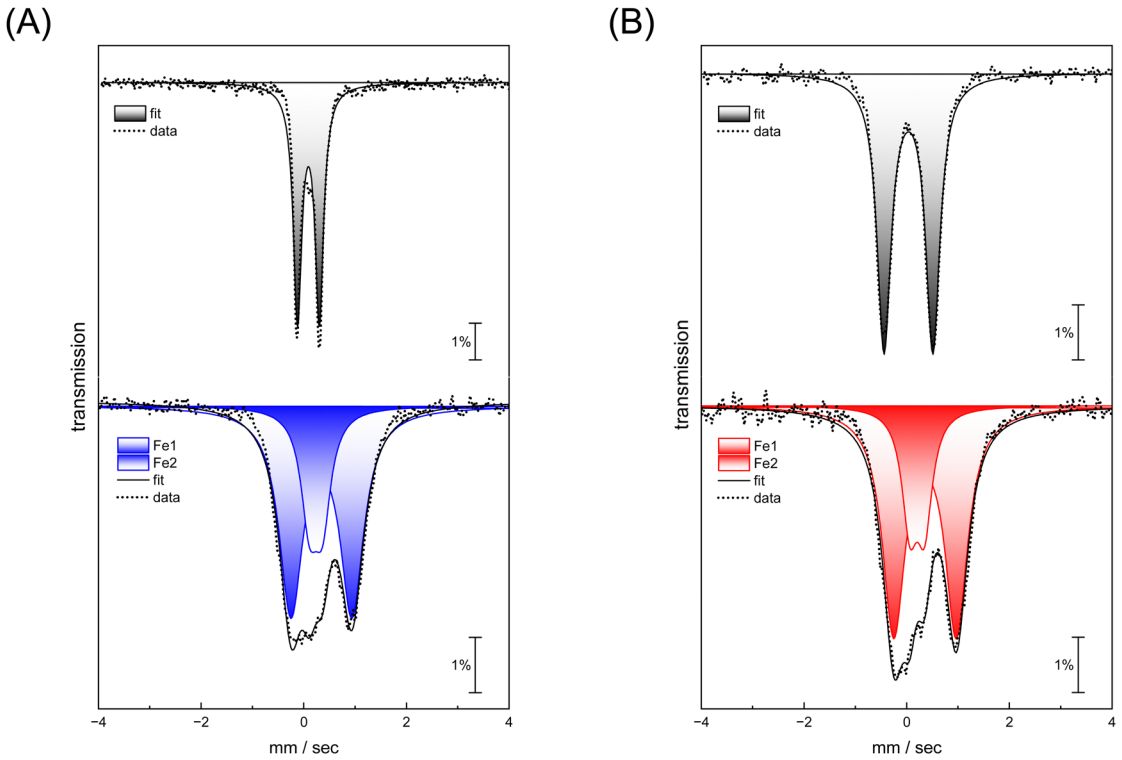

Fig. 5 (A) Mössbauer spectra of complex ADT_{CN} **[1]** and (B) PDT_{CN} **[2]** under anaerobic conditions (top traces) and recorded after purging the complexes with O_2 for 30 seconds each (lower traces, blue ADT_{CN} **[1]** and red ADT_{CN} **[2]**).

Table 2 Comparison of isomer shift and quadrupole splitting for complexes ADT_{CN} **[1]** and PDT_{CN} **[2]**

	[1]	[1]		[2]	[2]	
Model	$-O_2$	$+O_2$		$-O_2$	$+O_2$	
Iron	Fe1	Fe1	Fe2	Fe1	Fe1	Fe2
δ	0.037	0.238	0.345	0.035	0.204	0.358
ΔE_q	1.109	0.253	1.188	0.951	0.288	1.219

superoxide-binding state (H_{ox}–O_2) was trapped and suggested to be unreactive provided no further protonation occurs.[50]

Reaction of the complexes with O_2 in presence of protons.

As a proton-reducing enzyme, [FeFe]-hydrogenase cycles through various catalytic intermediates while shuttling protons. Moreover, the O_2 sensitivity significantly depends on the availability of protons at the H-cluster.[16,51] Therefore, the active site mimics were tested towards O_2 sensitivity in the presence of protons. Acids with varying strength were employed. Firstly, studies were carried out using acetic acid (pK_a = 23 in MeCN). The presence of one equivalent of acetic acid had no influence on the CO/CN^- band positions, which means that no protonation is observed, and both ADT_{CN} **[1]** and PDT_{CN} **[2]** react with O_2 in a similar manner as in the absence of protons (Fig. S6, ESI†).

Subsequently, the stronger acid *p*-toluene sulfonic acid (TsOH, pK_a = 8.3 in MeCN) was used. The FTIR spectra of complex **[1]** and **[2]** are dramatically influenced in the presence of TsOH. After addition of one equivalent of acid, a mean IR up-shift of 98 cm^{-1} (ν_{CO}) and 32 cm^{-1} (ν_{CN}) was recorded (Fig. 6(A), (B) and Table 3). This indicates protonation and/or oxidation of the complexes.[52,53] In variance to the reactions with O_2, note that both band intensity and band pattern are conserved in the absence and presence of protons. To further identify complex **[1]** and **[2]** in the presence of TsOH, ^1H NMR spectroscopy was performed. Fig. 6(C) shows high field ^1H signals at −19.15 ppm and −19.75 ppm for complex **[1]** and complex **[2]**, respectively, directly indicating formation of a bridging hydride ligand (μH) that differs from the terminal hydride at the H-cluster.[52,54] Both complexes show additional signals at −15.65 and −16.25 ppm indicating protonation of the CN^- ligands.[55] We note that the strong IR up-shift ligands may result from both protonation of the ligands and oxidation of the complexes due to hydride formation. In [FeFe]-hydrogenase, the CO ligands shift about ten times stronger than the CN^- ligands, *e.g.*, comparing the structurally conservative H_{ox} and H_{hyd} states.[56–58] The CO/CN^- shift ratio of only three observed here may reflect the stronger up-shift of the CN^- ligands upon protonation.

The catalytically relevant H-cluster state H_{hyd} carries a terminal hydride at Fe_d.[56–58] In variance, the bridging hydride geometry of complex **[1]** and **[2]** is comparable to H-cluster states H_{red} and H_{sred} where the diiron site formally adopts the Fe^{II}–Fe^{II} state and has been suggested to bind a μH ligand instead of a μCO ligand.[59–61] In these intermediates, [FeFe]-hydrogenase shows a prolonged resistance to O_2 and CO that we have explained by the presence of a fifth terminal ligand (CO

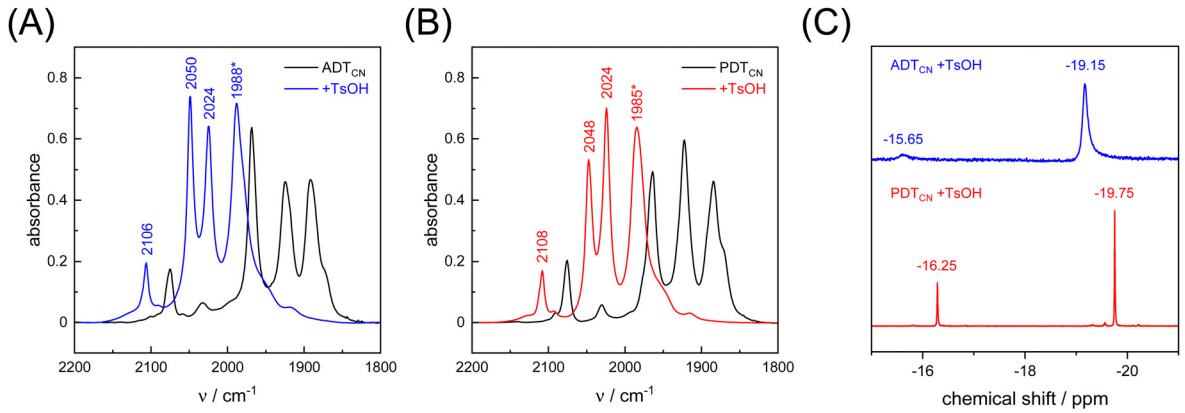

Fig. 6 FTIR spectra of (A) ADT_{CN} **[1]** and (B) PDT_{CN} **[2]** measured in the absence and presence of 1 equivalent of TsOH (black and blue/red traces). Asterisk: the bands at 1988 and 1985 cm^{-1} show a shoulder at 1977 and 1978 cm^{-1}, respectively. (C) ^1H NMR (CD_3CN, 400 MHz) spectra of ADT_{CN} **[1]** and PDT_{CN} **[2]** obtained upon reaction with 1 equivalent of TsOH. Signals at −19.15 and −19.75 stem from a μH ligand. Signals at −15.65 and −16.25 indicate protonation of the CN^- ligands.

Table 3 Observed IR band shifts. The reported values are before ($-H^+$) and after treatment with TsOH ($+H^+$). The mean shift of the CO ligands in **[1]** and **[2]** is 96 and 99 cm^{-1}, respectively

	[1]	[1]		[2]	[2]	
Model	$-H^+$	$+H^+$	Δ	$-H^+$	$+H^+$	Δ
νCO	1870	1977	**107**	1870	1978	**108**
νCO	1891	1988	**97**	1884	1985	**101**
νCO	1925	2024	**99**	1922	2024	**102**
νCO	1968	2050	**82**	1962	2048	**86**
νCN^-	2075	2106	**31**	2075	2108	**33**

or CN^-) occupying the open coordination site at Fe_d.[61,62] This model is not generally accepted, though. Under cryogenic conditions, ligand rotation is prohibited so that H_{red} and H_{sred} retain the μCO geometry and can be photoisomerized into H_{hyd}-like states.[63] It is conceivable that line broadening of the μCO band shows a stronger dependence on temperature than the terminal ligands, making the band "disappear" at room temperature.[64] This would explain the rather conservative, temperature-independent IR profile of the terminal ligands in H_{red} and H_{sred}.[59] However, the upshift of μCO in H_{red} and H_{sred} relative to H_{ox} is yet to explain,[63–65] and the presence of a third CO band between 1950–1960 cm^{-1} argues against a conservative μCO geometry.[60] Therefore, we suggest that complex **[1]** and **[2]** can serve as models for H_{red} and H_{sred}. After formation of the μH geometry, the model complexes display no further reactivity with O_2 and can be kept under aerobic conditions without further changes. Notably, these protonated states were also found to be resistant toward other oxidizing reagents such as H_2O_2 (Fig. S7, ESI†). Our observations highlight the similarities between the natural system and its respective mimic.[53,66]

Reaction of the complexes with hydrogen peroxide

Previous work on aerobic H-cluster deactivation suggested superoxide as an intermediate that requires further protonation. In aqueous solution, $^{\bullet}O_2^-$ is known to disproportionate into hydrogen peroxide (H_2O_2) and O_2 at physiologically relevant rates.[67] Therefore, H_2O_2 can be anticipated to be a major ROS involved in the decomposition of the H-cluster. First, we monitored the reactivity of complexes **[1–4]** with 30% H_2O_2 by IR spectroscopy. Fig. S8 (ESI†) show the differences in reactivity of complexes **[1]** and **[2]** with 2–10 equivalents of H_2O_2. Substochiometric amounts of H_2O_2 were found to result in very long reaction times (hours) and not considered. Again, ADT_{CN} **[1]** is more susceptible toward oxidation as it reacts with four equivalents of H_2O_2 while it takes at least six equivalents of H_2O_2 to convert PDT_{CN} **[2]** into an oxidized species. A quantitative titration was not attempted. The Mössbauer spectra observed for both complexes upon H_2O_2 treatment (Fig. S9, ESI†) are comparable to the ones observed after reaction with O_2 (Table S1, ESI†). Based on previous reports and our own data, di-ferrous complexes can be concluded.[68,69] Additionally, $ADT_{mono\text{-}CN}$ **[3]** degrades in presence of eight equivalents of H_2O_2, whereas no significant shifts in the IR spectra of $PDT_{mono\text{-}CN}$ **[4]** were observed (data not shown).

For both complex **[1]** and **[2]**, there are several possibilities of H_2O_2 to interact with the metal centers as well as with the adt or pdt ligand. Based on calculations by Reiher *et al.*, the reaction of the bridging sulfur atoms with H_2O_2 is most likely[43] but within the timeframe of our experiments, no oxygenation of the thiol groups were observed (Fig. S8, ESI†). Considering the large shifts in the FTIR spectra, a direct interaction of H_2O_2 with the iron sites seems plausible. Although the reaction with H_2O_2 should be independent of additional proton sources, we speculate that the diminished reactivity of the pdt-type complex **[2]** and **[4]** reflects the absence of the amine bridgehead that may stabilize an intermediate apical oxygen ligand.

Reaction of the enzyme with O_2 and H_2O_2

To probe the reactivity of complexes **[1–4]** as part of the H-cluster within [FeFe]-hydrogenase, we conducted aerobic deactivation experiments on *Cr*HydA1 matured with mimics **[1–4]** producing four cofactor variants namely *Cr*HydA1^{adt}, *Cr*HydA1^{pdt},

*Cr*HydA1$^{mono\text{-}adt}$, and *Cr*HydA1$^{mono\text{-}pdt}$. In preparation of the FTIR experiment, the enzymes were kept under an inert N_2 atmosphere to promote accumulation of the H_{ox} state, which was achieved for *Cr*HydA1^{adt} and *Cr*HydA1^{pdt} (Fig. S10, ESI†). However, for *Cr*HydA1$^{mono\text{-}adt}$ and *Cr*HydA1$^{mono\text{-}pdt}$ a mixture of unknown states was obtained (Fig. S11, ESI†) presumably due to different isomers of the model complexes **[3]** and **[4]** that were used to mature the apo-enzyme.[47,70] The CN^- ligands are important anchor points for the diiron site (Fig. 1). After oxidation of the enzymes, 20% O_2 v/v (or 5% H_2O_2 m/v) was introduced and changes of the H-cluster were monitored by *in situ* ATR FTIR spectroscopy.

In line with the results observed for the active site mimics the enzyme matured with ADT_{CN} **[1]** (*Cr*HydA1^{adt}, resembling wild-type enzyme) displayed faster degradation compared to *Cr*HydA1^{pdt} (Fig. 7(A)). FTIR difference spectra revealed a complete disintegration of the H-cluster in case of *Cr*HydA1^{adt} while a damaged cluster suggesting formation of a mono-metallic species with two CO and one CN^- ligands with bands at 1930, 1985, and 2095 cm^{-1} was observed for *Cr*HydA1^{pdt} (Fig. 8(A) and Fig. S10, ESI†). The 'survival' of an H-cluster fragment in CrHydA1^{pdt} is reminiscent of sensory [FeFe]-hydrogenases *Tam*HydS, where similar traces were observed after contact with O_2.[23] Just like *Cr*HydA1^{pdt} this hydrogenase shows a discontinued proton transfer pathway.[24,71] In case of *Cr*HydA1$^{mono\text{-}adt}$, the O_2 treatment revealed a significantly slower oxidation (Fig. S11, ESI†) much in agreement with an earlier report on *Cr*HydA1$^{mono\text{-}adt}$.[70] Notably, the H-cluster in *Cr*HydA1$^{mono\text{-}pdt}$ was resistant to O_2-induced oxidation as inferred from the largely unchanged FTIR spectra in Fig. S11 (ESI†).

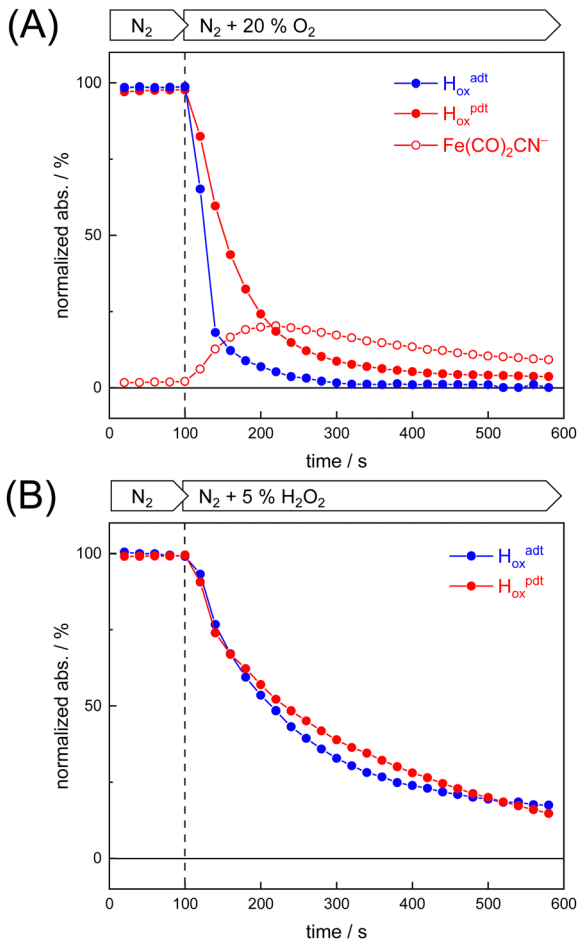

Fig. 7 Kinetics of oxidative damage to the H-cluster. The reaction of [FeFe]-hydrogenase *Cr*HydA1^{adt} and *Cr*HydA1^{pdt} with O_2 and H_2O_2 was monitored by *in situ* ATR FTIR spectroscopy. The normalized integral of all five H-cluster bands is plotted against time. (A) *Cr*HydA1^{adt} (H_{ox}, blue traces) was quickly deactivated in the presence of 20% O_2 v/v while cofactor variant *Cr*HydA1^{pdt} (H_{ox}, red traces) was deactivated notably slower and formed a $Fe(CO)_2CN^-$ intermediate (open red symbols). (B) No meaningful differences between *Cr*HydA1^{adt} and *Cr*HydA1^{pdt} were observed with 5% H_2O_2 m/v.

At lower frequencies, protonation and hydrogen-bonding changes shape the FTIR difference spectra. Fig. 8(B) highlights the deprotonation of glutamic acid residues E141 and E144 (negative bands at 1715 cm^{-1} and 1695 cm^{-1}) and the protonation of R148 (positive band at 1682 cm^{-1}) upon contact with O_2. These residues have been assigned in *Cr*HydA1 previously and correspond to E279, E282, and R286 in Fig. 1.[72,73] The reaction is potentially accompanied by protein structural changes (1675–1638 cm^{-1}). Surprisingly, both *Cr*HydA1^{adt} and *Cr*HydA1^{pdt} show very similar FTIR signatures, indicating proton transfer toward the H-cluster in the O_2 deactivation reaction. When scaled to the absorbance of the (negative) H_{ox} bands, the amino acid signals in *Cr*HydA1^{pdt} are half as intense as in *Cr*HydA1^{adt}. This results from hindered proton transfer in the pdt variant and can explain the observed differences deactivation kinetics (see Fig. S12, ESI† for the time-resolved evolution of FTIR difference spectra.).

Summing up, we found that the different *Cr*HydA1 cofactor variants follow the same O_2 degradation trend as observed with the model complexes. However, introduction of 5% H_2O_2 did not lead to a faster H-cluster degradation in *Cr*HydA1^{adt} as compared to *Cr*HydA1^{pdt} (Fig. 7(B)). Unlike model complexes **[1–4]** that show pronounced differences in H_2O_2 sensitivity amongst each other (Fig. S8, ESI†) the enzyme variants interact with H_2O_2 irrespective of the bridgehead ligand. Both enzymes reacted equally slow, arguably due to the smaller H_2O_2 concentration in the aerosol, and no traces of $Fe(CO)_2CN^-$ were observed.

Comparison between model complexes and enzyme

The differences in the rate of oxygen-induced degradation of ADT^{CN} **[1]** and PDT^{CN} **[2]** can be explained as follows. In both cases, O_2 initially interacts with the metal centers forming a metal–oxygen transient state. Based on the DFT calculations (Fig. S22 and Table S4, ESI†) and our data, a bridging peroxide dianion ligand ($\mu(O-)_2$) is most likely (Fig. S19 and S20, ESI†). This geometry is not optimal for proton transfer *via* the adt ligand and subsequent H_2O_2 formation. We speculate that this is the reason why even the most O_2-sensitive complex **[1]** is stable under air for several minutes. However, H_2O_2 formation is not suppressed completely, and our NMR data suggest that the CN^- ligands may assist in proton transfer toward

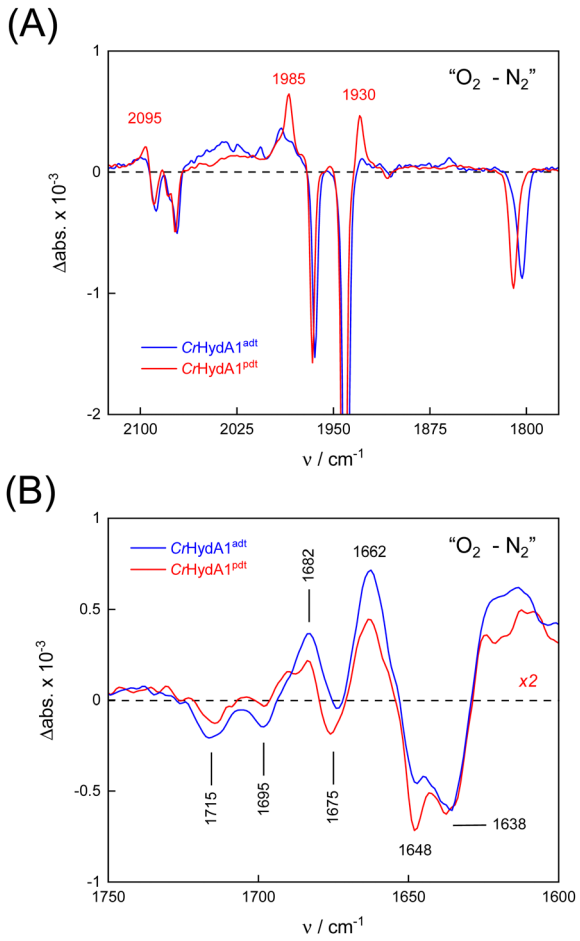

Fig. 8 FTIR difference spectra reveal details of the reaction with O_2. (A) In the CO/CN^- frequency regime of the H-cluster, O_2–N_2 spectra show the decrease of the H_{ox} state (negative bands). Note the accumulation of a $Fe(CO)_2CN^-$ intermediate exclusive to *Cr*HydA1^{pdt} (positive bands, red traces). (B) At lower frequencies, bands have been assigned to glutamic acid residues E141 and E144 (1715 and 1695 cm^{-1}) as well as arginine R148 (1682 cm^{-1}). Other feature may be related to protein structural changes. Note that the traces for *Cr*HydA1^{adt} and *Cr*HydA1^{pdt} are very similar.

μO_2^- (Fig. 6(C)). The later is true for complex **[2]** as well, which is why the increased O_2 stability of PDT^{CN} can only be explained by the lack of an internal hydrogen-boning donor.[42,74] The dithiolate ligand has limited effect on the electronic structure, as evidenced by the similar IR and Mössbauer spectra. Therefore, significant structural differences between complex **[1]** and **[2]** are excluded explaining the diverging kinetics. The mono-cyanide complexes **[3]** and **[4]** generally show higher Lewis acidity than the di-cyanide complexes **[1]** and **[2]**.[75] According to the model explained above, a lower pK_a of the ADT ligand can explain the resistance to aerobic deactivation in the mono-cyanide complexes. Similar arguments have been used to explain the necessity of CN^- ligands at the H-cluster.[76–80] Remarkably, our data on the diiron complexes suggest that the interaction with O_2 is not limited to the presence of an open binding site but rather is controlled by the ligand environment. The obtained results show that the bridgehead amine is not a mere spectator in oxygen-induced degradation but plays a crucial role in disintegration process.

A model consisting of O_2 reduction and protonation is applicable to [FeFe]-hydrogenase as well (Scheme 1). First, O_2 binds to the H-cluster in the H_{ox} state and is reduced to a superoxide ligand in the H_{ox}–O_2 state as characterized earlier.[50] The diiron site is oxidized from [Fe^{II}–Fe^{I}] to [Fe^{II}–Fe^{II}] in the process. In variance to the $\mu(O^-)_2$-binding complexes, the oxygen ligand is found in apical position in the enzyme; here, hydrogen-bonding with the adt ligand may promote the susceptibility to O_2 binding, reduction, and protonation thus slowing down the reaction velocity of *Cr*HydA1^{pdt}. Similar second coordination sphere effects have been observed for the formation and stabilization of the apical H^- ligand in the hydride state H_{hyd},[50,57,62] which cannot be accumulated in the pdt variant. In the second step, protonation and disproportionation of superoxide to H_2O_2 will demand an additional superoxide radical ($^{\bullet}O_2^-$). We speculate that this may stem from a second population of enzyme in the H_{ox}–O_2 state; such ligand transfer is common in [FeFe]-hydrogenase, *e.g.*, in the formation of the H_{ox}–CO state ("cannibalization").[81] Oxidation of $^{\bullet}O_2^-$ in the disproportionation reaction produces O_2, which may re-bind the intact H-cluster. For *Cr*HydA1^{pdt} and its parent complex PDT_{CN} **[2]**, the absence of a hydrogen-bonding donor impedes further ROS formation, hence a slower response towards O_2 is observed (Fig. 4 and 7). This observation in agreement with electrochemical O_2 reduction experiments by Dey *et al.*, where the formation of a catalytic peroxide species critically depends on hydrogen-bonding with an adt-type ligand.[36]

Reacting *Cr*HydA1^{adt} and *Cr*HydA1^{pdt} with H_2O_2 directly (Fig. 7(B)) allows bypassing the need for the explicit protonation step necessary in O_2-induced deactivation. We emphasize that these results agree with superoxide as an intermediate species in O_2-induced deactivation. Scheme 1 depicts how H_2O_2 formation may produce an unstable H-cluster species in the +4 state, not protected by a ligand in apical position at Fe_d. Eventually, H_2O_2 will continue to disintegrate the H-cluster and other metal centers in the enzyme.[15–18]

Conclusions

We have probed active site mimics of [FeFe]-hydrogenase and the respective enzyme variants toward O_2 deactivation and their reactivity with various reactive oxygen species (ROS). Our results show that in the case of the model complexes, the primary deleterious interaction occurs at the iron center(s). Concomitant O_2 binding and oxidation of the diiron site is required. Thereafter, a rapid degenerative pathway follows, which is influenced by the nature of the bridgehead ligand. The ADT_{CN} complex **[1]**, featuring an amine bridgehead, exhibits higher response towards O_2, while the PDT_{CN} complex **[2]**, with a methylene bridgehead, shows reduced reactivity. Furthermore, the reactivity of mono- and di-cyanide substituted complexes correlates with increased O_2 and H_2O_2 susceptibility,

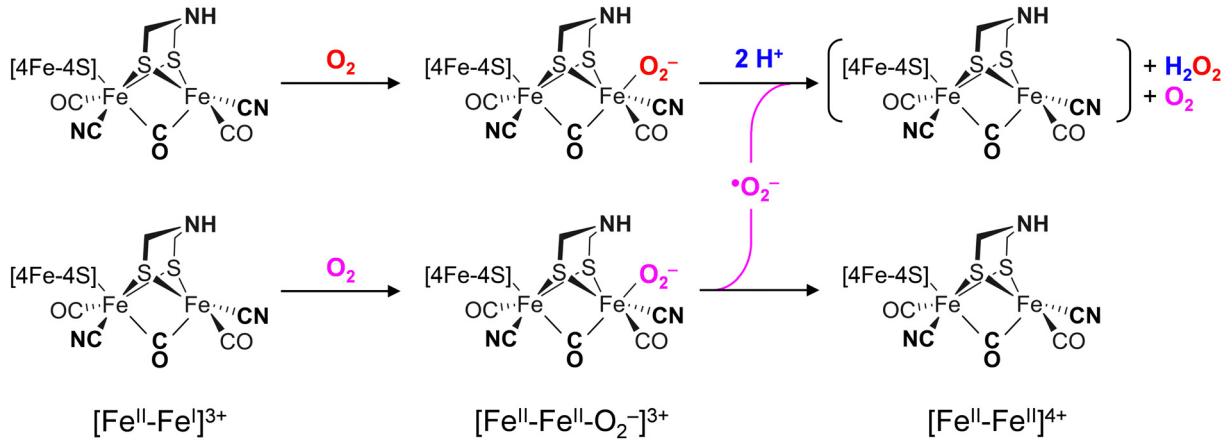

Scheme 1 Binding and reduction of O_2 at the H-cluster in the [Fe^{II}–Fe^{I}] state (H_{ox}) produces the [Fe^{II}–Fe^{II}–O_2^-] state (H_{ox}–O_2) stabilized by hydrogen bonding between ligands adt and O_2^- (dashed lines). Protonation and disproportionation of superoxide leads to H_2O_2 formation and regeneration of O_2. We presume that the [Fe^{II}–Fe^{II}] state is unstable and will continue decaying.

presumably due to a decrease in acidity proportional to the number of cyanide ligands.[75]

In [FeFe]-hydrogenase fine tuning *via* the amine bridgehead and the diatomic ligands of the H-cluster is necessary for the supreme catalytic activity. This includes proton transfer, the formation of a frustrated Lewis pair between adt and Fe_d, hydrogen bonding between CN^- and protein (Fig. 1), and other "outer" coordination sphere effects.[9] However, this unique arrangement comes at the expense of O_2 sensitivity where electron transfer precedes proton transfer resulting in the sub-stochiometric production of harmful H_2O_2 (Scheme 1). While [FeFe]-hydrogenases treat O_2 essentially like a proton, [NiFe]-hydrogenases are reversibly inhibited by O_2[82] or have evolved to fully reduce O_2 to two equivalents of H_2O, *e.g.*, in Knallgas bacteria.[25–29] Some [FeFe]-hydrogenases adopt inhibited states in the presence of O_2[20–24] but from a physiological perspective, [FeFe]-hydrogenase may fail at O_2 tolerance due to the lack of evolutionary pressure.[83] Our study now establishes reactivity patterns of [FeFe]-hydrogenase mimics, offering insights into the initial steps of oxygen deactivation in the enzyme. We propose a model in which O_2 binds to the H-cluster, is reduced to an apical superoxide ligand and reacts to H_2O_2 upon proton transfer and disproportionation. Such species then continue to deactivate the [FeFe]-hydrogenase.[15–18]

Remarkably, the active site mimics react with protons resulting in a bridging hydride state (Fe^{II}–μH–Fe^{II}), which is unresponsive towards O_2 and H_2O_2. This observation agrees with the enhanced O_2-stability of certain H-cluster intermediates[62] where a μH ligand is formed at the reduced diiron site and an apical CO ligand slows down aerobic deactivation.[59–61] The identification of an O_2-stable Fe^{II}–μH–Fe^{II} state may inspire the design of new O_2 tolerant catalysts.

Abbreviations

adt	Azadithiolate
pdt	Propanedithiolate
ROS	Reactive oxygen species
FTIR	Fourier-transform infrared
NMR	Nuclear magnetic resonance
EPR	Electron paramagnetic resonance
DFT	Density functional theory

Author contributions

SY synthesized complexes, performed spectroscopy, and wrote the manuscript; RH produced and activated the enzyme; EBB performed DFT calculations; MR analyzed DFT calculations; TH reviewed the manuscript; UPA analyzed data and wrote the manuscript; STS performed spectroscopy, analyzed data, and wrote the manuscript.

Data availability

The data supporting this article have been included as part of the ESI.†

Conflicts of interest

There are no conflicts to declare.

Acknowledgements

The authors acknowledge Melanie Heghmanns and Müge Kasanmascheff for assistance with the EPR measurements of the samples. STS acknowledges Joachim Heberle for providing access to his laboratory and spectrometers at Freie Universität Berlin. We thank Moritz Senger for fruitful discussions. SY gratefully acknowledges the German Academic Exchange Service (DAAD) for a scholarship. This work was supported by the Deutsche Forschungsgemeinschaft (DFG, RO 5688/1, AP242/12-1, and STR 1554/5-1). This work was likewise supported by the Fraunhofer Internal Programs under Grant No. Attract 097-602175

and the DFG under Germany's Excellence Strategy – EXC-2033 – Projektnummer 390677874 "RESOLV".

References

1 International Energy Agency, Global Hydrogen Review 2021, OECD, 2021.
2 B.-F. M. for E. A. and C. Action, "The National Hydrogen Strategy," can be found under **https://www.bmwk.de/Redaktion/EN/Publikationen/Energie/the-national-hydrogen-strategy.html**, n.d.
3 D. Siegmund, S. Metz, V. Peinecke, T. E. Warner, C. Cremers, A. Grevé, T. Smolinka, D. Segets and U.-P. Apfel, *JACS Au*, 2021, **1**, 527–535.
4 M. Yue, H. Lambert, E. Pahon, R. Roche, S. Jemei and D. Hissel, *Renewable Sustainable Energy Rev.*, 2021, **146**, 111180.
5 W. Lubitz, H. Ogata, O. Rüdiger and E. Reijerse, *Chem. Rev.*, 2014, **114**, 4081–4148.
6 C. Madden, M. D. Vaughn, I. Díez-Pérez, K. A. Brown, P. W. King, D. Gust, A. L. Moore and T. A. Moore, *J. Am. Chem. Soc.*, 2012, **134**, 1577–1582.
7 J. T. Kleinhaus, F. Wittkamp, S. Yadav, D. Siegmund and U.-P. Apfel, *Chem. Soc. Rev.*, 2021, **50**, 1668–1784.
8 J. A. Birrell, P. Rodríguez-Maciá, E. J. Reijerse, M. A. Martini and W. Lubitz, *Coord. Chem. Rev.*, 2021, **449**, 214191.
9 S. T. Stripp, B. R. Duffus, V. Fourmond, C. Léger, S. Leimkühler, S. Hirota, Y. Hu, A. Jasniewski, H. Ogata and M. W. Ribbe, *Chem. Rev.*, 2022, **122**, 11900–11973.
10 H. Tai, S. Hirota and S. T. Stripp, *Acc. Chem. Res.*, 2021, **54**, 232–241.
11 J. Esselborn, N. Muraki, K. Klein, V. Engelbrecht, N. Metzler-Nolte, U.-P. Apfel, E. Hofmann, G. Kurisu and T. Happe, *Chem. Sci.*, 2016, **7**, 959–968.
12 A. Kubas, C. Orain, D. De Sancho, L. Saujet, M. Sensi, C. Gauquelin, I. Meynial-Salles, P. Soucaille, H. Bottin, C. Baffert, V. Fourmond, R. B. Best, J. Blumberger and C. Léger, *Nat. Chem.*, 2017, **9**, 88–95.
13 M. Mohammadi and H. Vashisth, *J. Phys. Chem. B*, 2017, **121**, 10007–10017.
14 J. Cohen, K. Kim, P. King, M. Seibert and K. Schulten, *Structure*, 2005, **13**, 1321–1329.
15 M. T. Stiebritz and M. Reiher, *Inorg. Chem.*, 2009, **48**, 7127–7140.
16 J. Esselborn, L. Kertess, U.-P. Apfel, E. Hofmann and T. Happe, *J. Am. Chem. Soc.*, 2019, **141**, 17721–17728.
17 S. T. Stripp, G. Goldet, C. Brandmayr, O. Sanganas, K. A. Vincent, M. Haumann, F. A. Armstrong and T. Happe, *Proc. Natl. Acad. Sci. U. S. A.*, 2009, **106**(41), 17331–17336.
18 K. D. Swanson, M. W. Ratzloff, D. W. Mulder, J. H. Artz, S. Ghose, A. Hoffman, S. White, O. A. Zadvornyy, J. B. Broderick, B. Bothner, P. W. King and J. W. Peters, *J. Am. Chem. Soc.*, 2015, **137**, 1809–1816.
19 G. Goldet, C. Brandmayr, S. T. Stripp, T. Happe, C. Cavazza, J. C. Fontecilla-Camps and F. A. Armstrong, *J. Am. Chem. Soc.*, 2009, **131**, 14979–14989.
20 S. Morra, M. Arizzi, F. Valetti and G. Gilardi, *Biochemistry*, 2016, **55**, 5897–5900.
21 M. Winkler, J. Duan, A. Rutz, C. Felbek, L. Scholtysek, O. Lampret, J. Jaenecke, U.-P. Apfel, G. Gilardi, F. Valetti, V. Fourmond, E. Hofmann, C. Léger and T. Happe, *Nat. Commun.*, 2021, **12**, 756.
22 H. Land, M. Senger, G. Berggren and S. T. Stripp, *ACS Catal.*, 2020, **10**, 7069–7086.
23 H. Land, A. Sekretareva, P. Huang, H. J. Redman, B. Németh, N. Polidori, L. S. Mészáros, M. Senger, S. T. Stripp and G. Berggren, *Chem. Sci.*, 2020, **11**, 12789–12801.
24 P. R. Cabotaje, K. Walter, A. Zamader, P. Huang, F. Ho, H. Land, M. Senger and G. Berggren, *ACS Catal.*, 2023, **13**, 10435–10446.
25 J. A. Cracknell, A. F. Wait, O. Lenz, B. Friedrich and F. A. Armstrong, *Proc. Natl. Acad. Sci. U. S. A.*, 2009, **106**, 20681–20686.
26 J. Fritsch, P. Scheerer, S. Frielingsdorf, S. Kroschinsky, B. Friedrich, O. Lenz and C. M. T. Spahn, *Nature*, 2011, **479**, 249–252.
27 S. Frielingsdorf, J. Fritsch, A. Schmidt, M. Hammer, J. Löwenstein, E. Siebert, V. Pelmenschikov, T. Jaenicke, J. Kalms, Y. Rippers, F. Lendzian, I. Zebger, C. Teutloff, M. Kaupp, R. Bittl, P. Hildebrandt, B. Friedrich, O. Lenz and P. Scheerer, *Nat. Chem. Biol.*, 2014, **10**, 378–385.
28 P. Wulff, C. C. Day, F. Sargent and F. A. Armstrong, *Proc. Natl. Acad. Sci. U. S. A.*, 2014, **111**, 6606–6611.
29 L. Lauterbach and O. Lenz, *J. Am. Chem. Soc.*, 2013, **135**, 17897–17905.
30 H. Li and T. B. Rauchfuss, *J. Am. Chem. Soc.*, 2002, **124**, 726–727.
31 J. L. Stanley, T. B. Rauchfuss and S. R. Wilson, *Organometallics*, 2007, **26**, 1907–1911.
32 A. L. Cloirec, S. C. Davies, D. J. Evans, D. L. Hughes, C. J. Pickett, S. P. Best and S. Borg, *Chem. Commun.*, 1999, 2285–2286.
33 E. J. Lyon, I. P. Georgakaki, J. H. Reibenspies and M. Y. Darensbourg, *Angew. Chem., Int. Ed.*, 1999, **38**, 3178–3180.
34 L. Mond and C. Langer, *J. Chem. Soc., Trans.*, 1891, **59**, 1090–1093.
35 W. Hieber and J. Gruber, *Z. Anorg. Allg. Chem.*, 1958, **296**, 91–103.
36 S. Dey, A. Rana, D. Crouthers, B. Mondal, P. K. Das, M. Y. Darensbourg and A. Dey, *J. Am. Chem. Soc.*, 2014, **136**, 8847–8850.
37 V. C.-C. Wang, C. Esmieu, H. J. Redman, G. Berggren and L. Hammarström, *Dalton Trans.*, 2020, **49**, 858–865.
38 J. Windhager, R. A. Seidel, U.-P. Apfel, H. Görls, G. Linti and W. Weigand, *Chem. Biodiversity*, 2008, **5**, 2023–2041.
39 T. Liu, B. Li, M. L. Singleton, M. B. Hall and M. Y. Darensbourg, *J. Am. Chem. Soc.*, 2009, **131**, 8296–8307.
40 M. Y. Darensbourg and W. Weigand, *Eur. J. Inorg. Chem.*, 2011, 994–1004.
41 J. A. Imlay, *Mol. Microbiol.*, 2006, **59**, 1073–1082.
42 A. R. Finkelmann, M. T. Stiebritz and M. Reiher, *Inorg. Chem.*, 2014, **53**, 11890–11902.

43 M. K. Bruska, M. T. Stiebritz and M. Reiher, *J. Am. Chem. Soc.*, 2011, **133**, 20588–20603.
44 M. Schieber and N. S. Chandel, *Curr. Biol.*, 2014, **24**, R453–R462.
45 L. Kertess, F. Wittkamp, C. Sommer, J. Esselborn, O. Rüdiger, E. J. Reijerse, E. Hofmann, W. Lubitz, M. Winkler, T. Happe and U.-P. Apfel, *Dalton Trans.*, 2017, **46**, 16947–16958.
46 C. Esmieu and G. Berggren, *Dalton Trans.*, 2016, **45**, 19242–19248.
47 J. F. Siebel, A. Adamska-Venkatesh, K. Weber, S. Rumpel, E. Reijerse and W. Lubitz, *Biochemistry*, 2015, **54**, 1474–1483.
48 F. Gloaguen, J. D. Lawrence, M. Schmidt, S. R. Wilson and T. B. Rauchfuss, *J. Am. Chem. Soc.*, 2001, **123**, 12518–12527.
49 S. Detoni and D. Hadzi, *Spectrochim. Acta*, 1956, **11**, 601–608.
50 S. Mebs, R. Kositzki, J. Duan, L. Kertess, M. Senger, F. Wittkamp, U.-P. Apfel, T. Happe, S. T. Stripp, M. Winkler and M. Haumann, *Biochim. Biophys. Acta, Bioenerg.*, 2018, **1859**, 28–41.
51 J. Noth, R. Kositzki, K. Klein, M. Winkler, M. Haumann and T. Happe, *Sci. Rep.*, 2015, **5**, 13978.
52 X. Zhao, I. P. Georgakaki, M. L. Miller, J. C. Yarbrough and M. Y. Darensbourg, *J. Am. Chem. Soc.*, 2001, **123**, 9710–9711.
53 F. Gloaguen, J. D. Lawrence, T. B. Rauchfuss, M. Bénard and M.-M. Rohmer, *Inorg. Chem.*, 2002, **41**, 6573–6582.
54 S. Rumpel, E. Ravera, C. Sommer, E. Reijerse, C. Farès, C. Luchinat and W. Lubitz, *J. Am. Chem. Soc.*, 2018, **140**, 131–134.
55 A. Jablonskytė, J. A. Wright and C. J. Pickett, *Dalton Trans.*, 2010, **39**, 3026.
56 D. W. Mulder, Y. Guo, M. W. Ratzloff and P. W. King, *J. Am. Chem. Soc.*, 2017, **139**, 83–86.
57 M. Winkler, M. Senger, J. Duan, J. Esselborn, F. Wittkamp, E. Hofmann, U.-P. Apfel, S. T. Stripp and T. Happe, *Nat. Commun.*, 2017, **8**, 16115.
58 E. J. Reijerse, C. C. Pham, V. Pelmenschikov, R. Gilbert-Wilson, A. Adamska-Venkatesh, J. F. Siebel, L. B. Gee, Y. Yoda, K. Tamasaku, W. Lubitz, T. B. Rauchfuss and S. P. Cramer, *J. Am. Chem. Soc.*, 2017, **139**, 4306–4309.
59 S. T. Stripp, S. Mebs and M. Haumann, *Inorg. Chem.*, 2020, **59**, 16474–16488.
60 M. Haumann and S. T. Stripp, *Acc. Chem. Res.*, 2018, **51**, 1755–1763.
61 S. Mebs, M. Senger, J. Duan, F. Wittkamp, U.-P. Apfel, T. Happe, M. Winkler, S. T. Stripp and M. Haumann, *J. Am. Chem. Soc.*, 2017, **139**, 12157–12160.
62 J. Duan, S. Mebs, K. Laun, F. Wittkamp, J. Heberle, T. Happe, E. Hofmann, U.-P. Apfel, M. Winkler, M. Senger, M. Haumann and S. T. Stripp, *ACS Catal.*, 2019, **9**, 9140–9149.
63 C. Lorent, S. Katz, J. Duan, C. J. Kulka, G. Caserta, C. Teutloff, S. Yadav, U.-P. Apfel, M. Winkler, T. Happe, M. Horch and I. Zebger, *J. Am. Chem. Soc.*, 2020, **142**, 5493–5497.
64 J. A. Birrell, V. Pelmenschikov, N. Mishra, H. Wang, Y. Yoda, K. Tamasaku, T. B. Rauchfuss, S. P. Cramer, W. Lubitz and S. DeBeer, *J. Am. Chem. Soc.*, 2020, **142**, 222–232.
65 M. W. Ratzloff, J. H. Artz, D. W. Mulder, R. T. Collins, T. E. Furtak and P. W. King, *J. Am. Chem. Soc.*, 2018, **140**, 7623–7628.
66 F. Gloaguen, J. D. Lawrence and T. B. Rauchfuss, *J. Am. Chem. Soc.*, 2001, **123**, 9476–9477.
67 Y. Sheng, I. A. Abreu, D. E. Cabelli, M. J. Maroney, A.-F. Miller, M. Teixeira and J. S. Valentine, *Chem. Rev.*, 2014, **114**, 3854–3918.
68 F. Roncaroli, E. Bill, B. Friedrich, O. Lenz, W. Lubitz and M.-E. Pandelia, *Chem. Sci.*, 2015, **6**, 4495–4507.
69 A. S. Pereira, P. Tavares, I. Moura, J. J. G. Moura and B. H. Huynh, *J. Am. Chem. Soc.*, 2001, **123**, 2771–2782.
70 M. Lorenzi, J. Gellett, A. Zamader, M. Senger, Z. Duan, P. Rodríguez-Maciá and G. Berggren, *Chem. Sci.*, 2022, **13**, 11058–11064.
71 A. Fasano, H. Land, V. Fourmond, G. Berggren and C. Léger, *J. Am. Chem. Soc.*, 2021, **143**, 20320–20325.
72 M. Senger, V. Eichmann, K. Laun, J. Duan, F. Wittkamp, G. Knör, U.-P. Apfel, T. Happe, M. Winkler, J. Heberle and S. T. Stripp, *J. Am. Chem. Soc.*, 2019, **141**, 17394–17403.
73 J. Duan, M. Senger, J. Esselborn, V. Engelbrecht, F. Wittkamp, U.-P. Apfel, E. Hofmann, S. T. Stripp, T. Happe and M. Winkler, *Nat. Commun.*, 2018, **9**, 4726.
74 A. Kubas, D. De Sancho, R. B. Best and J. Blumberger, *Angew. Chem., Int. Ed.*, 2014, **53**, 4081–4084.
75 A. Nayek, S. Dey, S. Patra, A. Rana, P. N. Serrano, S. J. George, S. P. Cramer, S. G. Dey and A. Dey, *Chem. Sci.*, 2024, **15**, 2167–2180.
76 F. Wang, M. Wang, X. Liu, K. Jin, W. Dong and L. Sun, *Dalton Trans.*, 2007, 3812–3819.
77 F. Wang, M. Wang, X. Liu, K. Jin, W. Dong, G. Li, B. Åkermark and L. Sun, *Chem. Commun.*, 2005, 3221–3223.
78 G. Eilers, L. Schwartz, M. Stein, G. Zampella, L. de Gioia, S. Ott and R. Lomoth, *Chem. – Eur. J.*, 2007, **13**, 7075–7084.
79 Ö. F. Erdem, M. Stein, S. Kaur-Ghumaan, E. J. Reijerse, S. Ott and W. Lubitz, *Chem. – Eur. J.*, 2013, **19**, 14566–14572.
80 T. B. Rauchfuss, *Acc. Chem. Res.*, 2015, **48**, 2107–2116.
81 W. Roseboom, A. L. De Lacey, V. M. Fernandez, E. C. Hatchikian and S. P. J. Albracht, *J. Biol. Inorg. Chem.*, 2006, **11**, 102–118.
82 K. A. Vincent, A. Parkin, O. Lenz, S. P. J. Albracht, J. C. Fontecilla-Camps, R. Cammack, B. Friedrich and F. A. Armstrong, *J. Am. Chem. Soc.*, 2005, **127**, 18179–18189.
83 S. Morra, *Front. Microbiol.*, 2022, 13.

